AGU PUBLICATIONS

JGR

Journal of Geophysical Research: Atmospheres

RESEARCH ARTICLE
10.1002/2017JD026716

Key Points:
- An oxygen isotope record from southeast Greenland revealed that isotope-enabled models reproduce well the interannual and intraannual variations
- The similar intraannual variations enable us to construct a precise age scale by fitting oxygen isotope data to a simulated template record
- The reconstructed snow accumulation rate shows an increasing trend over the past 54 years, with a dominant contribution of autumn snow

Correspondence to:
R. Uemura and Y. Iizuka,
ruemura@sci.u-ryukyu.ac.jp;
iizuka@lowtem.hokudai.ac.jp

Citation:
Furukawa, R., Uemura, R., Fujita, K., Sjolte, J., Yoshimura, K., Matoba, S., & Iizuka Y. (2017). Seasonal-scale dating of a shallow ice core from Greenland using oxygen isotope matching between data and simulation. *Journal of Geophysical Research: Atmospheres*, *122*, 10,873–10,887. https://doi.org/10.1002/2017JD026716

Received 28 FEB 2017
Accepted 3 AUG 2017
Accepted article online 15 SEP 2017
Published online 26 OCT 2017

Seasonal-Scale Dating of a Shallow Ice Core From Greenland Using Oxygen Isotope Matching Between Data and Simulation

Ryoto Furukawa[1], Ryu Uemura[2], Koji Fujita[3], Jesper Sjolte[4], Kei Yoshimura[5], Sumito Matoba[1], and Yoshinori Iizuka[1]

[1]Institute of Low Temperature Science, Hokkaido University, Sapporo, Japan, [2]Department of Chemistry, Biology, and Marine Science, Faculty of Science, University of the Ryukyus, Nishihara, Japan, [3]Graduate School of Environmental Studies, Nagoya University, Nagoya, Japan, [4]Department of Geology, Quaternary Science, Lund University, Lund, Sweden, [5]Institute of Industrial Science, The University of Tokyo, Tokyo, Japan

Abstract A precise age scale based on annual layer counting is essential for investigating past environmental changes from ice core records. However, subannual scale dating is hampered by the irregular intraannual variabilities of oxygen isotope ($\delta^{18}O$) records. Here we propose a dating method based on matching the $\delta^{18}O$ variations between ice core records and records simulated by isotope-enabled climate models. We applied this method to a new $\delta^{18}O$ record from an ice core obtained from a dome site in southeast Greenland. The close similarity between the $\delta^{18}O$ records from the ice core and models enables correlation and the production of a precise age scale, with an accuracy of a few months. A missing $\delta^{18}O$ minimum in the 1995/1996 winter is an example of an indistinct $\delta^{18}O$ seasonal cycle. Our analysis suggests that the missing $\delta^{18}O$ minimum is likely caused by a combination of warm air temperature, weak moisture transport, and cool ocean temperature. Based on the age scale, the average accumulation rate from 1960 to 2014 is reconstructed as 1.02 m yr^{-1} in water equivalent. The annual accumulation rate shows an increasing trend with a slope of 3.6 mm yr^{-1}, which is mainly caused by the increase in the autumn accumulation rate of 2.6 mm yr^{-1}. This increase is likely linked to the enhanced hydrological cycle caused by the decrease in Arctic sea ice area. Unlike the strong seasonality of precipitation amount in the ERA reanalysis data in the southeast dome region, our reconstructed accumulation rate suggests a weak seasonality.

1. Introduction

A precise relationship between the age and depth of an ice core is essential for interpreting paleoenvironmental proxies preserved in ice (e.g., Meese et al., 1997). For ice cores, the depth versus age relationship is determined by counting annual layers of the concentrations of chemical species and isotopic composition. In Greenland, inland dome ice cores have countable annual layers (Greenland Ice Sheet Project 2 (GISP2)) (Alley et al., 1997; Meese et al., 1997, and NGRIP: Svensson et al., 2008; Vinther et al., 2010), which can be identified by the annual fluctuations in soluble impurities, electrical conductivity, and oxygen and hydrogen isotopes in the ice ($\delta^{18}O$ and δD). Additional time markers provide additional constraints to tune the age-depth relationships. Typical time markers are peaks in acid concentrations from volcanic eruption layers (Hammer et al., 1980) and peaks in β-activity from nuclear bomb test layers (Holdsworth et al., 1984).

The precision of annual layer counting depends on whether annual layers are clearly identifiable in the isotope and chemical records. Meese et al. (1997) showed that the uncertainly in ages was 2% for the GISP2 core during the Holocene. In low snow accumulation sites, the isotopic composition of surface snow is also affected by isotopic exchanges with ambient atmospheric water vapor in between precipitation events (Steen-Larsen et al., 2014). Postdepositional effects also include diffusion of the stable isotope compositions of ice (Hoshina et al., 2014, 2016; Town et al., 2008) and snowmelt (Koerner, 1997). Therefore, the high accumulation rate, which minimizes postdepositional effects, is a key factor for precise layer counting.

The majority of the dating uncertainty for annual timescale is caused by erroneous interpretation of uncertain annual layers (Rasmussen et al., 2006). For subannual time scale, the intraannual variations (i.e., peaks within a year and/or missing peaks) in the $\delta^{18}O$ cycle makes it difficult to determine the age scale with sufficient precision. A promising tool to solve this fundamental problem is isotope-enabled climate models (e.g., Risi

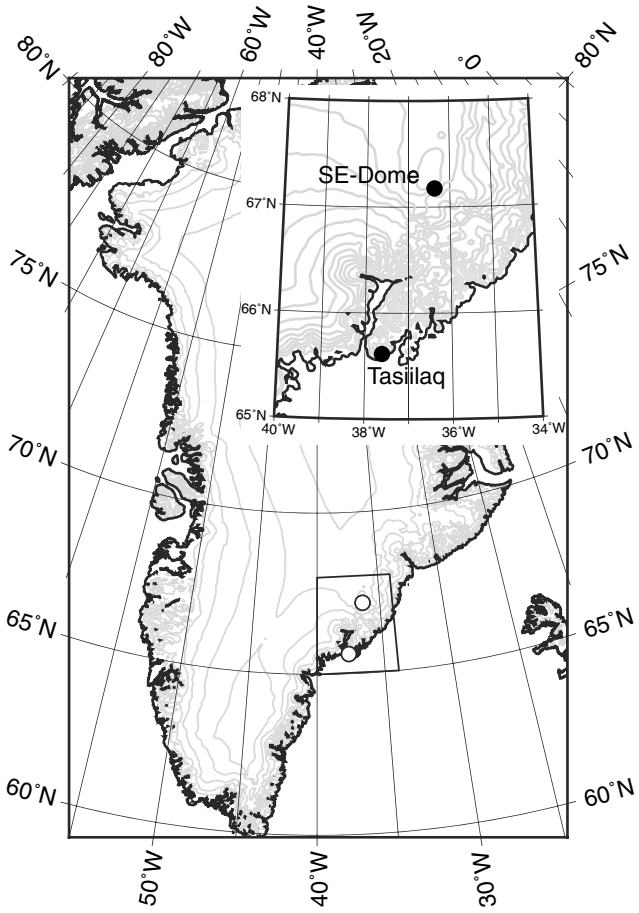

Figure 1. Map showing locations of the SE-Dome and a meteorological station Tasiilaq.

et al., 2012; Sjolte et al., 2011; Yoshimura et al., 2008). The isotope models simulate isotopic variations in precipitation, for example, at a drilling site, which can be used as a template for matching the ice core isotope profile. Although the matching can be carried out only within the period covered by reanalysis data, high-precision dating should be useful for investigation of other proxies preserved in ice cores such as volcanic sulfates (Plummer et al., 2012), chemical composition of sulfate aerosols particles (Iizuka et al., 2012), black carbon (McConnell et al., 2007), isotope compositions of nitrate (Geng et al., 2014), and radiogenic aerosols (Berggren et al., 2009), extending to the period before instrumental observations of these chemical components began.

Here we demonstrate a precise dating method of a shallow ice core using output from isotope models as a template record. We used a new $\delta^{18}O$ record from a 90.45 m depth ice core obtained from southeast Greenland (hereafter, SE-Dome) (Iizuka et al., 2016). The SE-Dome ice core is especially suitable to test this approach because of its distinctly high accumulation rate, estimated to be ~1.0 m yr^{-1} (water equivalent ice accumulation) (Iizuka et al., 2017). This guarantees a paleo-environmental reconstruction of high-temporal resolution with minimum postdepositional effects. We used two isotopic models, REMO-iso and iso-GSM. REMO-iso is a mesoscale climate model fitted with stable water isotope diagnostics nudged to follow observed weather patterns (Sjolte et al., 2011), while iso-GSM is a global three-dimensional stable water isotope model (Yoshimura et al., 2008). The clear covariation between the data and models enables us to establish subannual age-markers. The precision of the age scale is evaluated using the tritium and sulfate age-markers and the seasonal variation of sea salt. We will discuss the detailed variations in the isotope compositions over the past 54 years, with a focus on the anomalously warm winter in 1995/1996. Furthermore, the precise age scale enables us to reconstruct the seasonal changes in the snow accumulation rate at SE-Dome, suggesting that the accumulation is uniform in all seasons and that a long-term increasing trend in annual and autumn accumulation rates exists over the past 54 years.

2. Materials and Methods

2.1. SE-Dome Ice Core

A 90.45 m depth ice core was obtained at SE-Dome in southeast Greenland (67.18°N, 36.37°W, 3170 m above sea level (asl); Figure 1). The annual mean temperature is −20.9°C based on the 20 m depth firn temperature (Iizuka et al., 2016). The accumulation rate is estimated to be ~1.0 m yr^{-1} in water equivalents between 1963 and 2015 based on tritium and electrical conductivity measurements (Iizuka et al., 2017). This is the highest accumulation rate among the domes on the polar ice sheets, at 4 times that of typical inland Greenlandic core sites, and 30 times that of typical inland Antarctic core sites.

2.2. Isotope and Ion Measurements

The SE-Dome ice core was cut every 50 mm of depth in a cold room at the Institute of Low Temperature Science (ILTS), Hokkaido University, Japan. The upper part of the core, above 12.5 m, was cut every 100 mm of depth because of its low firn density. The surface of each sample was then decontaminated using a clean ceramic knife in a cold clean room (class 10000) and placed into a clean polyethylene bottle. The samples were melted at room temperature in a clean room.

The stable oxygen isotope composition of water was measured using a water isotope analyzer (Picarro L2120-i, Picarro Inc., Santa Clara, CA, USA) with an evaporating device (Picarro, A0212 vaporizer) at the

Table 1
Average Values and Standard Deviations of the $\delta^{18}O$ Profiles From iso-GSM, REMO-iso, and SE-Dome Ice Core

	Iso-GSM	REMO-iso	SE-Dome core
Average of $\delta^{18}O$	−19.45	−21.55	−27.26
$\delta^{18}O$ standard deviation	2.38	3.52	3.32
Period	1979–2015	1959–2001	1956–2014

ILTS. The analytical precision of $\delta^{18}O$ was 0.08‰. In total, 1637 samples were measured along the 90.45 m length of the ice core, with an average resolution of 55 mm.

The concentrations of Cl^-, SO_4^{2-}, and Na^+ were measured by ion chromatography (Thermo Scientific, ICS-2100; Dionex CS-12A column with 20 mM methanesulfonic acid eluent for cations; and Dionex AS-14A column with 23 mM NaOH eluent for anions). The analytical precision of the ion concentrations was 10%. Large peaks in the ion concentrations were carefully checked. First, the peaks were identified by comparison with the data from two adjacent samples. Then, if the 3-point running standard deviation was significantly large ($>3\sigma$), the detected outliers were remeasured in a new ice sample from the same depth. A full discussion of the ion concentrations can be found in another paper. In this paper, the Cl^-, SO_4^{2-}, and Na^+ concentrations were only used to evaluate the age scale.

2.3. Isotope General Circulation Models

REMO-iso is a regional climate model with isotope diagnostics included in the hydrological cycle (Sturm et al., 2005). The model was setup with a 0.5° rotated horizontal grid (approximately 55 km) with 19 vertical hybrid levels and run over the Greenland region, while being nudged spectrally toward the wind field of the ERA-40 reanalysis data set (Sjolte et al., 2011). The model run covers the period 1959–2001.

The iso-GSM is an atmospheric general circulation model (GCM), into which stable water isotopes are incorporated (Yoshimura, 2015; Yoshimura et al., 2008). The model uses the T62 horizontal resolution (approximately 200 km) and 28 vertical levels up to 10 hPa (approximately 30 km altitude), and the temporal resolution of the output is 6 h. The model was spectrally nudged toward the wind and temperature fields from the National Centers for Environmental Prediction (NCEP), Department of Energy Reanalysis 2 (Kanamitsu et al., 2002), in addition to being forced with the prescribed sea surface temperature (SST) and sea ice data from an NCEP analysis, from 1979 to present. The general reproducibility of the model on daily to interannual timescales has been well evaluated by comparing it with the isotope ratio of precipitation (Uemura et al., 2012; Yoshimura et al., 2008), the isotope ratio of vapor from satellite and in situ measurements (Okazaki et al., 2015; Uemura et al., 2008; Wei et al., 2016; Yoshimura et al., 2011), and isotopic proxies (Yoshimura, 2015).

From both models, we used the isotope data of precipitation for the grid box nearest to the SE-Dome. Although the site is close to ocean, the grid box is land in the two models. Model elevations are 2352 m and 1663 m for REMO-iso and iso-GSM, respectively, with the actual elevation of the core site being 3170 m. The data for two isotope models cover different periods, 1959–2001 for REMO-iso and 1979–2015 and for iso-GSM. During the overlapping period (1979–2001), monthly $\delta^{18}O$ values showed high correlation between two models ($R^2 = 0.41$), although the average $\delta^{18}O$ value of REMO-iso is 2.0‰ lower than that of iso-GSM (Table 1). This $\delta^{18}O$ offset is likely due to a difference in the model site elevations caused by the different spatial resolution of the models and characteristics of each model.

We constructed an averaged model $\delta^{18}O$ profile by averaging the normalized $\delta^{18}O$ profiles of each model as only the $\delta^{18}O$ variability is needed for matching the SE core data. The normalized $\delta^{18}O$ data, $\delta^{18}O_{nor}$, were obtained as follows:

$$\delta^{18}O_{nor} = \left(\delta^{18}O_{raw} - \delta^{18}O_{ave}\right)/\sigma_{18O}, \quad (1)$$

where σ_{18O} is the standard deviation of the data and the subscripts "raw" and "ave" indicate the raw and averaged values, respectively. The averaged model $\delta^{18}O$ profile, $\delta^{18}O_{model}$, was obtained by averaging the $\delta^{18}O_{nor}$ records of REMO-iso and iso-GSM.

2.4. Dating of Ice and Reconstruction of Snow Accumulation

The SE-Dome $\delta^{18}O$ and $\delta^{18}O_{model}$ variations were matched by selecting manually 170 tie points from 0.8 to 86.5 m depth using AnalySeries software (Paillard et al., 1996). This matching provides a relationship between the depth (ice core) and date (model). Then, the SE-Dome core age scale based on the isotope composition

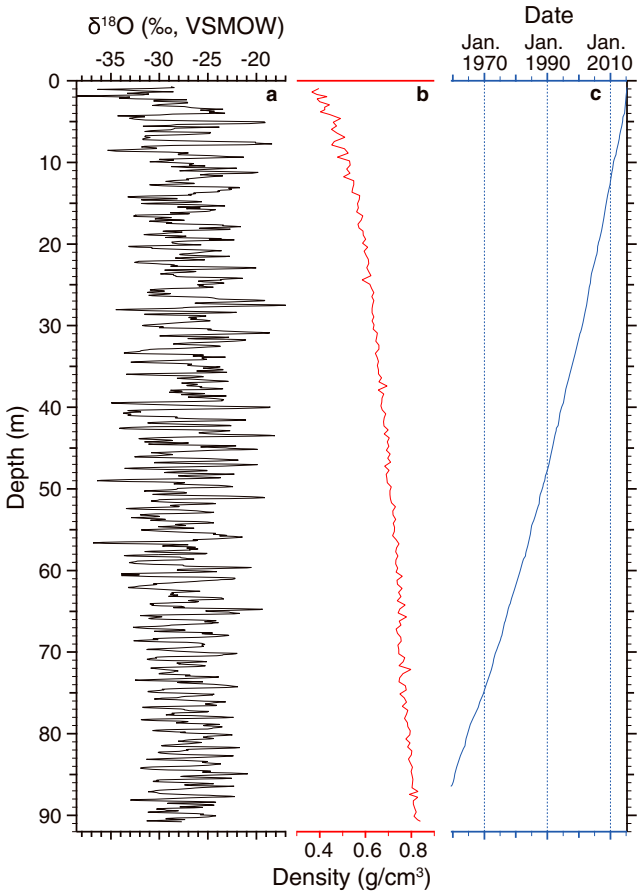

Figure 2. Isotope and density profiles of the SE-Dome ice core. (a) $\delta^{18}O$ of ice (black), (b) density of ice (red; from Iizuka et al., 2017), and (c) date of the ice based on the SEIS 2016 age scale (blue).

(SE dome ISotope age scale; hereafter, SEIS2016 age scale) was constructed by linearly interpolating between the points.

To obtain the annual accumulation rate, the depth was resampled at 1 year intervals based on the SEIS2016 age scale during 1960–2014. The depth of 1 year interval indicates the annual accumulation rate in snow equivalents. Then, the snow accumulation rate in water-equivalent depth was calculated by multiplying snow density (Figure 2). In the same way, the seasonal accumulation rates were obtained based with seasonal boundaries of 1 March, 1 June, 1 September, and 1 December.

2.5. ERA-40 and ERA-Interim Reanalysis Data

To evaluate climate records in the SE-Dome ice core, we made a long continuous reanalysis record by combining the ERA-40 (1958–2001) and ERA-Interim (1979–2014; hereafter, ERA-I) reanalysis data sets produced by the European Centre for Medium-Range Weather Forecasts (ECMWF) (Dee et al., 2011; Uppala et al., 2005). The combined record of the two products (hereafter, ERA-40-I) was prepared as follows. A linear regression of the monthly variables (temperature and precipitation) of ERA-40 and ERA-I for the overlapping period 1979–2001 was written as

$$v_I = a\, v_{40} + b, \tag{2}$$

where v_I and v_{40} are the monthly variables of ERA-I and ERA-40, respectively. For temperature, the coefficients were $a = 0.958$ and $b = -0.305$ ($R^2 = 0.997$, $p < 0.001$, root-mean-square error (RMSE) = 0.60°C). For precipitation, the coefficients are $a = 1.382$ and $b = 0.000$ ($R^2 = 0.884$, $p < 0.001$, RMSE = 32.2 mm month^{-1}). The daily mean air temperature at SE-Dome was estimated from the temperatures at two geopotential heights bounding/containing the elevation of the site (3170 m asl) in the manner of Sakai et al. (2015). Then, the linearly calibrated ERA-40 data (1958–1978) were connected to the ERA-I data (1979–2014).

In addition, to analyze the winter conditions in 1995/1996 (section 3.3.), the anomalies of the winter mean (December, January, and February) of the 2 m air temperature, SST, and wind at 850 hPa were also calculated from the long-term mean (1979–2015) in the ERA-I data.

3. Results and Discussion

3.1. Isotope Variations From the Ice Core and Models

Figure 2 shows the $\delta^{18}O$ and snow density profiles of the SE-Dome ice core with depth. The $\delta^{18}O$ values vary from −38.5 to −17.0‰. Maxima and minima in $\delta^{18}O$ are observed with a wavelength of about 1.5 m, suggesting that the ice core preserves an approximately 60 yearlong record. Figure 3 shows the $\delta^{18}O_{model}$ and $\delta^{18}O$ in the SE-Dome core with visual matching points between them on the SEIS2016 age scale. The seasonal variations in the $\delta^{18}O$ records are very similar. In fact, the monthly $\delta^{18}O$ data from the SE-Dome ice core and two models covary with correlation coefficients (r) of 0.66 ($p < 0.01$) for REMO-iso and 0.69 ($p < 0.01$) for iso-GSM. Most years show clear summer (maximum) and winter (minimum) signals for the $\delta^{18}O$ values, except the shallow minimum for the winter 1984/1985 and nearly no minimum during the winter 1995/1996. The subannual scale variations are also similar for the modeled and measured $\delta^{18}O$. For example, double peaks are recognized in both time series during some summer maxima in $\delta^{18}O$ (1981, 1987, 1990, and 1992). These results demonstrate that the precise age scale of a shallow ice core can be established by matching with the output from isotope models.

3.2. Evaluation of the Dating Uncertainty

Figure 4 shows the SE-Dome $\delta^{18}O$ variations with age markers on the SEIS2016 age scale. Two age markers, tritium and SO_4^{2-}, provide independent tie points for the age scale. First, a tritium content peak is observed from 81.38 to 81.88 m (Iizuka et al., 2017). This depth interval corresponds to 1963 (from January to

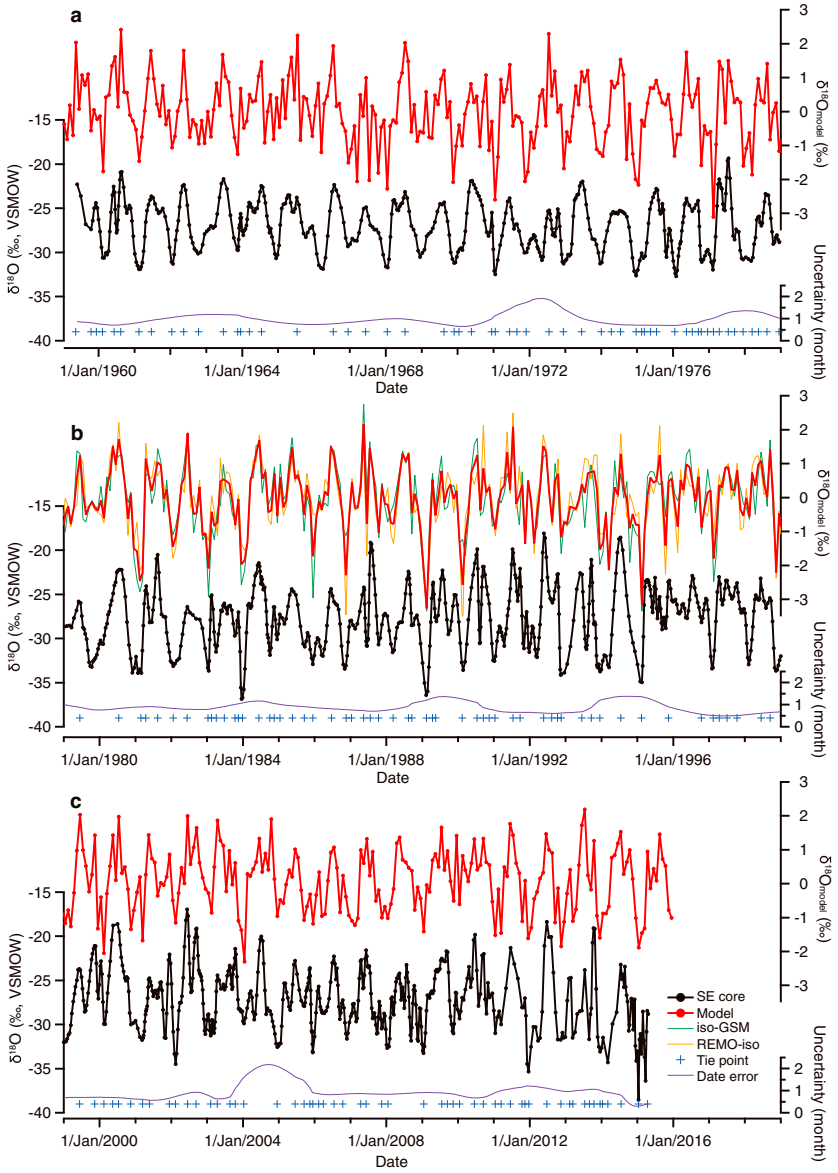

Figure 3. Matching between the $\delta^{18}O$ variations from the ice core and model. (a) SE-Dome ice core $\delta^{18}O$ (black) and $\delta^{18}O_{model}$ (red) during 1959–1978, (b) 1979–1998, and (c) 1999–2014. The blue crosses show the 170 tie points used for $\delta^{18}O$ matching. The purple lines indicate the 95% confidence limit of the age scale. The $\delta^{18}O$ data of iso-GSM (green) and REMO-iso (yellow) were also shown in **b**.

December) in SEIS2016 age (Figure 4a), consistent with a major peak in β-activity in 1963 caused by nuclear bomb testing (Clausen & Hammer, 1988; Holdsworth et al., 1984). The 1963 peak is also consistent with the ^{239}Pu records at D4 and Summit ice cores (Arienzo et al., 2016), although the ^{239}Pu records show maxima in 1962 at northern sites (NEEM and TUNU; Arienzo et al., 2016). Second, the Pinatubo eruption, the largest volcanic event of the 20th century, which occurred on 15 June 1991, can be identified in the high SO_4^{2-} peak at 43.49 m in the SE-Dome ice core. This depth corresponds to May 1992 in SEIS2016 age (Figure 4b). The time lag between the eruption and the SO_4^{2-} peak is attributable to the time required for the volcanic gas to be oxidized and transported to the northern high-latitude region through the stratosphere. An atmospheric transport model estimated that the maximum aerosol optical depth reached its maximum in the latter half of 1992 in the 70°S region (Gao et al., 2008). Another atmospheric chemistry simulation showed that the maximum aerosol optical depth occurred around the spring of 1992 (Dhomse et al., 2014). Therefore, the accuracy of the SEIS2016 age scale is also supported by the SO_4^{2-} peak in 1992, associated with the Pinatubo eruption.

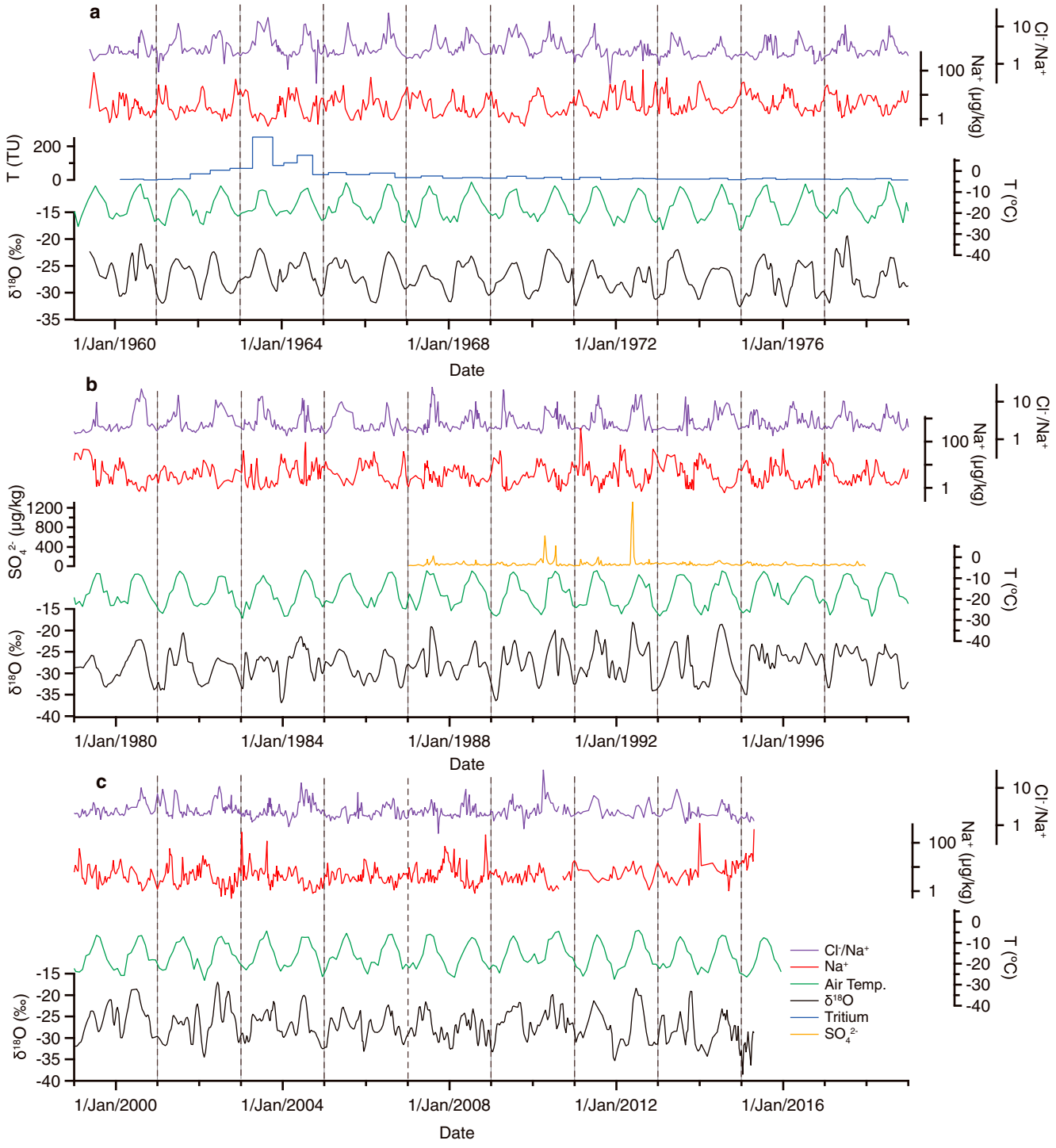

Figure 4. Time series of $\delta^{18}O$ and age markers in the SE-Dome core with ERA-40-I air temperatures. (a) SE-Dome core $\delta^{18}O$ (black), Na^+ concentration (red), Cl^-/Na^+ ratio (purple), and tritium concentration (blue; from Iizuka et al., 2017) during 1959–1978. The green line indicates the monthly mean ERA-40-I temperature at the SE-Dome elevation. (b) The same as in Figure 4a but during 1979–1998, and the SO_4^{2-} concentration (yellow) is also shown. (c) The same as in Figure 4a but during 1999–2014.

The uncertainty in the age scale on a subannual time scale can be evaluated indirectly using the concentrations of sea-salt ions, Na^+ and Cl^-. The Na^+ concentration in Greenland is highest in winter due to a high sea-salt content of aerosols and/or late winter cyclonic storms (Whitlow et al., 1992). The Cl^-/Na^+ ratio, on the other hand, is maximal in summer because of the preferential removal of Na^+ in aerosols relative to

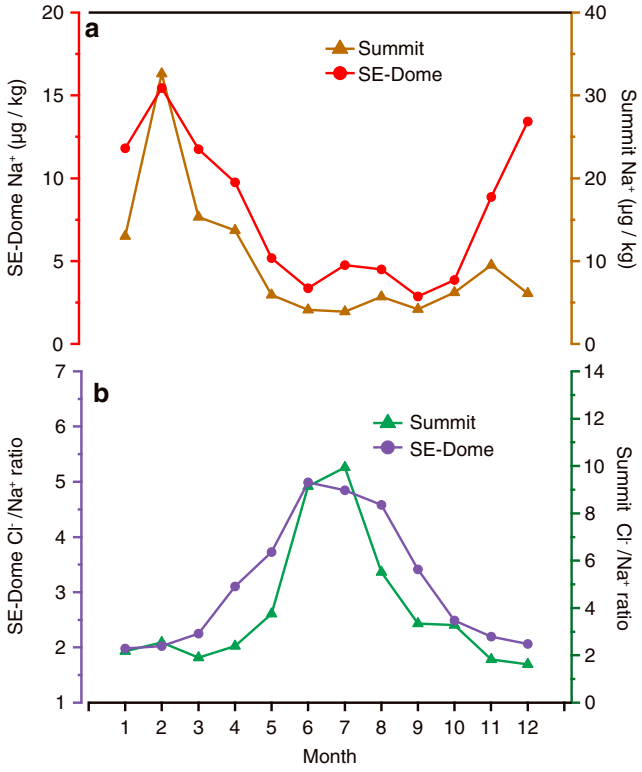

Figure 5. Comparison of the ion data from SE-Dome with the surface snow observation at Summit. (a) Monthly average of Na^+ concentration in the SE-Dome ice core over 1959–2015 (red), and the Na^+ concentration (brown) in surface snow at Summit, Greenland (Dibb et al., 2007). (b) The same as in Figure 5a but for the Cl^-/Na^+ ratio in the SE-Dome ice core (purple) and surface snow (green) at Summit (Dibb et al., 2007).

gaseous Cl (Whitlow et al., 1992). This seasonal marker is used to date shallow ice cores from Summit (Geng et al., 2014). The precise timing of peak months was determined by a daily sampling of surface snow at Summit over 1997–1998 and 2000–2002 (Dibb et al., 2007). The snow data revealed a Na^+ maximum in February and Cl^-/Na^+ maximum in July (Figure 5).

The Na^+ and Cl^-/Na^+ records from the SE-Dome ice core are shown in Figure 4. Generally, Na^+ peaks in winter, and Cl^-/Na^+ peaks in summer. Monthly averaged data of the Na^+ concentration and Cl^-/Na^+ were calculated based on the record from 1959 to 2015 (Figure 5). The highest concentration month for a Na^+ is February, and relatively higher concentrations are observed from November to March. The highest month for a Cl^-/Na^+ peak is June, and higher values are found from May to August. The Na^+ and Cl^-/Na^+ peak months and their distribution patterns in the SE-Dome core are markedly coincident with the Na^+ and Cl^-/Na^+ observation at the Summit site (Dibb et al., 2007) (Figure 5) In fact, the peak months in the ice core and daily snow data agree within a few months. This result suggests that the SEIS2016 age scale is precise enough to reconstruct seasonal scale variations.

Notably, several anomalous Na^+ peaks were found in summer months (Figure 4). These anomalous peaks do not indicate incorrect dating, but rather show the short irregular fluctuations in the Na^+ concentration. For example, in 1972, the Na^+ concentration was at a maximum in August (110 μg/kg), but the second highest value was detected in March (40 μg/kg) (Figure 4a). The presence of such intraannual peaks is an obstacle in dating based on ion concentration alone. In general, for annual layer identification, such two closely spaced peaks can be identified by irregular annual layer thicknesses (Rasmussen et al., 2006). The isotope matching dating technique, as presented here, overcomes this challenge by using a template $\delta^{18}O$ profile generated from isotope simulations. The isotope ratio also has intraannual peaks, which will be discussed in the next section.

The varying uncertainty from section to section was calculated by using an algorithm (Scholz & Hoffmann, 2011) based on a Monte Carlo simulation fitting ensembles of straight lines to subsets of the age data. To calculate a confidence limit, an age determination error at each tie point should be assigned. We assumed that the error at each tie point is ±1 month because most of intratannual $\delta^{18}O_{model}$ peaks, selected for tie points, consist of three data points (Figure 3). In most periods, the 95% confidence limit is around 1 month (average ± 0.9 month). There are, however, larger uncertainties where the number of tie points is small (Figure 3). The largest uncertainty was found in October 2004 (±2.4 month). Thus, we estimate that the precision of the SEIS2016 age scale is within a few months.

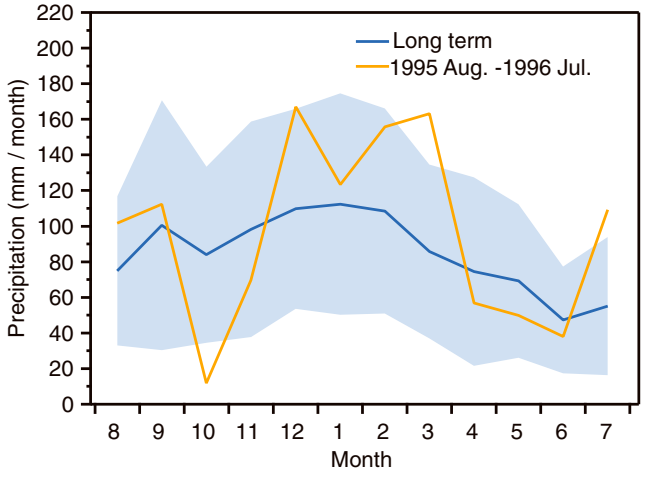

Figure 6. Monthly precipitation in the SE-Dome region based on ERA-I. (a) Long-term mean value during 1979–2015 (blue) with the standard deviation (blue shading). (b) Precipitation data from August 1995 to July 1996 (orange).

3.3. Missing Isotope Minimum in the 1995/1996 Winter

The $\delta^{18}O$ record of the SE-Dome ice core shows seasonal variations, and the winter values are 3–5‰ lower than the annual average (Figure 4). In the winter between 1995 and 1996, however, $\delta^{18}O$ does not exhibit a minimum and shows a nearly flat plateau (Figure 4b). It is difficult to recognize such nonsinusoidal variations as a winter minimum by counting annual layers. The $\delta^{18}O$ matching method

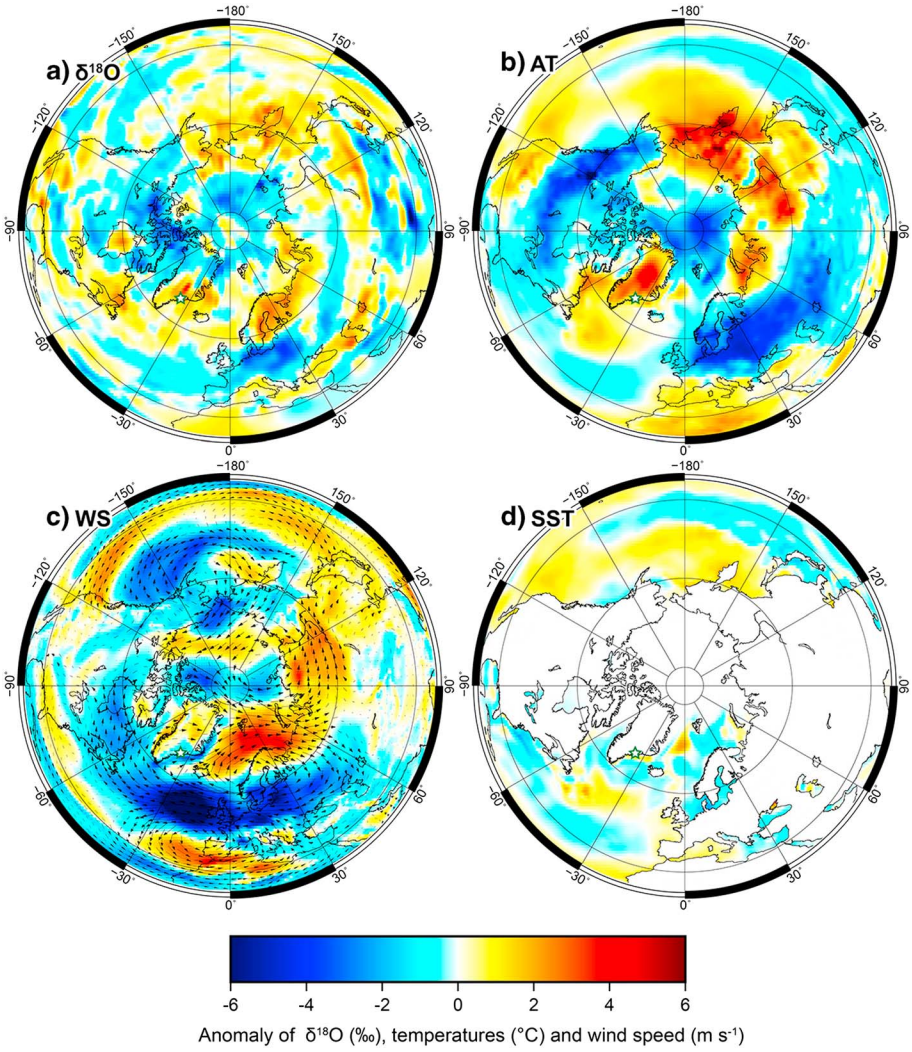

Figure 7. Anomaly of the winter (December to February) climate pattern during 1995/1996 against long-term mean (1979–2015) with the location of SE-Dome site (green star). Anomaly of (a) $\delta^{18}O$ of precipitation from iso-GSM, (b) 2 m air temperature (AT) from ERA-I, (c) wind speed (WS) at the 850 hPa pressure level from ERA-I, and (d) SST from ERA-I.

enabled us to detect such an anomalous year; in fact, the $\delta^{18}O_{model}$ record also shows a flat variation during the 1995/1996 winter (Figure 3). The missing isotopic minimum would not have been caused by a deficit of low-$\delta^{18}O$ snow in winter because the seasonal accumulation rate based on the ERA-I precipitation data for the 1995/1996 winter is greater than that of a normal winter (Figure 6).

The iso-GSM data depict a positive anomaly of $\delta^{18}O$ in precipitation around the SE core site (Figure 7a), suggesting that this phenomenon occurred regionally in south-eastern Greenland. The 1995/1996 winter season featured recurring and unusual weather patterns throughout the middle latitudes of the Northern Hemisphere, which were associated with an abnormal planetary-scale pattern of storm tracks and westerly winds that extended from the North Pacific Ocean eastward through Eurasia (Climate Prediction Center, 1996). During the winter 1995/1996 the air temperature at 2 m height in Greenland shows an anomaly of +4°C (Figure 7b). This warming partly explains the high $\delta^{18}O$ value. However, considering the slope of the regression line between the SE-Dome $\delta^{18}O$ and ERA40-I temperature (0.41‰/°C, $r^2 = 0.46$, $p < 0.01$), the 4°C warming corresponds to only a 1.6‰ increase in $\delta^{18}O$, which is insufficient to explain the ~3–5‰ higher value during the 1995/1996 winter.

Figure 7c shows the wind speed anomaly at the 850 hPa pressure level, where the westerly wind was significantly reduced over the North Atlantic Ocean. This negative anomaly of the 850 hPa wind suggests that the

Table 2
Correlation Coefficients (r) of the Seasonal SE-Dome Core $\delta^{18}O$ Values Against the ERA-40-I Air Temperature and Against the NAO Index

	Annual $\delta^{18}O$	Spring(MAM) $\delta^{18}O$	Summer(JJA) $\delta^{18}O$	Autumn(SON) $\delta^{18}O$	Winter(DJF) $\delta^{18}O$
ERA-40-I air temperature	0.46***	0.29**	0.28**	0.37***	0.66***
NAO index	−0.31**	−0.16 (ns)	−0.11 (ns)	−0.23*	−0.49***

Note. ns: not significant.
*$p < 0.1$. **$p < 0.05$. ***$p < 0.01$.

origin of the water vapor for the SE-core site was closer than usual, which would lead to a shorter transport distance for water vapor and result in less depleted $\delta^{18}O$ values. Moreover, the SST anomaly indicates cooling around the ocean offshore Greenland (Figure 7d). This low SST causes a smaller temperature difference between the SE-core site and moisture source and may lead to higher $\delta^{18}O$ values because of the smaller amount of rainout during Rayleigh fractionation (Dansgaard, 1964). In summary, the high $\delta^{18}O$ value in the 1995/1996 winter was likely caused by a combination of warmer air temperature at SE-Dome, reduced wind speed in the North Atlantic region, and lower SST offshore of Greenland.

3.4. Correlation Between $\delta^{18}O$ and Air Temperature

The SE-Dome $\delta^{18}O$ record correlates well with the ERA-40-I air temperature during 1960–2014. The correlations are statistically significant for not only the annual average but also the variations in each season for spring (March-April-May (MAM)), summer (June-July-August (JJA)), autumn (September-October-November (SON)), and winter (December-January-February (DJF)) (Table 2). The covariation of the annual $\delta^{18}O$ and air temperature from 1960 to 2014 (Figure 8) suggests that the SE-Dome $\delta^{18}O$ value can be used as a proxy of air temperature. For seasonal variations, the winter $\delta^{18}O$ and temperature show a general decreasing trend from 1963 to 1994, increase to higher values in 1994–1996, and subsequently appear to maintain these high values (Figure 8). The winter $\delta^{18}O$ record has a particularly high correlation with the winter air-temperature ($r = 0.66$, $p < 0.001$) (Figure 8).

In central and south Greenland, $\delta^{18}O$ is strongly influenced by the North Atlantic Oscillation (NAO) (Vinther et al., 2010; White et al., 1997), while a weaker influence was detected at the northern site, NEEM (Masson-Delmotte et al., 2015). The correlation between SE-Dome $\delta^{18}O$ and the NAO index is summarized in Table 2. Here we used the principal-component based indices of the NAO (Hurrell, 2003). The highest correlation was found between the winter $\delta^{18}O$ values and winter NAO index ($r = -0.49$), as also found in the first principal component signal from seven Greenland ice cores (Vinther et al., 2003). Figure 8 shows the time series of the winter $\delta^{18}O$ values and winter NAO index. The records show very similar interannual trends as found in the winter temperature record. These winter correlations suggest that the winter temperature in the SE-Dome region is controlled by the Icelandic Low.

It should be noted that the correlation between ERA-40-I and SE-Dome $\delta^{18}O$ is partly a result of our dating method and the characteristics of the models. Figure 9 illustrates the intercorrelation between the SE-Dome core, isotope models, and ERA reanalysis data. The air temperature and $\delta^{18}O$ are correlated in the model ($r = 0.61$ for REMO-iso, $r = 0.68$ for iso-GSM), and the temperature variations in the isotope models are also well correlated with the reanalysis data. Consequently, the correlation between the temperature and SE-Dome $\delta^{18}O$ was expected because the SE-Dome $\delta^{18}O$ was matched to $\delta^{18}O_{model}$. On the other hand, the high correlation between the SE-Dome $\delta^{18}O$ and temperature did not depend entirely on the dating method. In fact, the coefficient of determination between the ice core $\delta^{18}O$ and model $\delta^{18}O$ values, $R^2 = 0.44$–0.47, indicates that only about half of the variance of the model $\delta^{18}O$ can be explained by the ice core observations. The remaining variations are caused by the uncertainty in the reanalyzed meteorological data and the physical and isotope-fractionation processes described in the models. In this context, the observed correlation between the SE-Dome core $\delta^{18}O$ and ERA-40-I temperature should be interpreted as evidence of the $\delta^{18}O$-temperature correlation simulated in the models and of the seasonal-scale precision of SEIS2016 age scale.

3.5. Snow Accumulation During 1960–2014

The SEIS2016 age scale allows us to evaluate the past variations in snow accumulation at the SE-Dome core site. Unlike the relationship of $\delta^{18}O$ versus temperature, the accumulation is independent of the precipitation

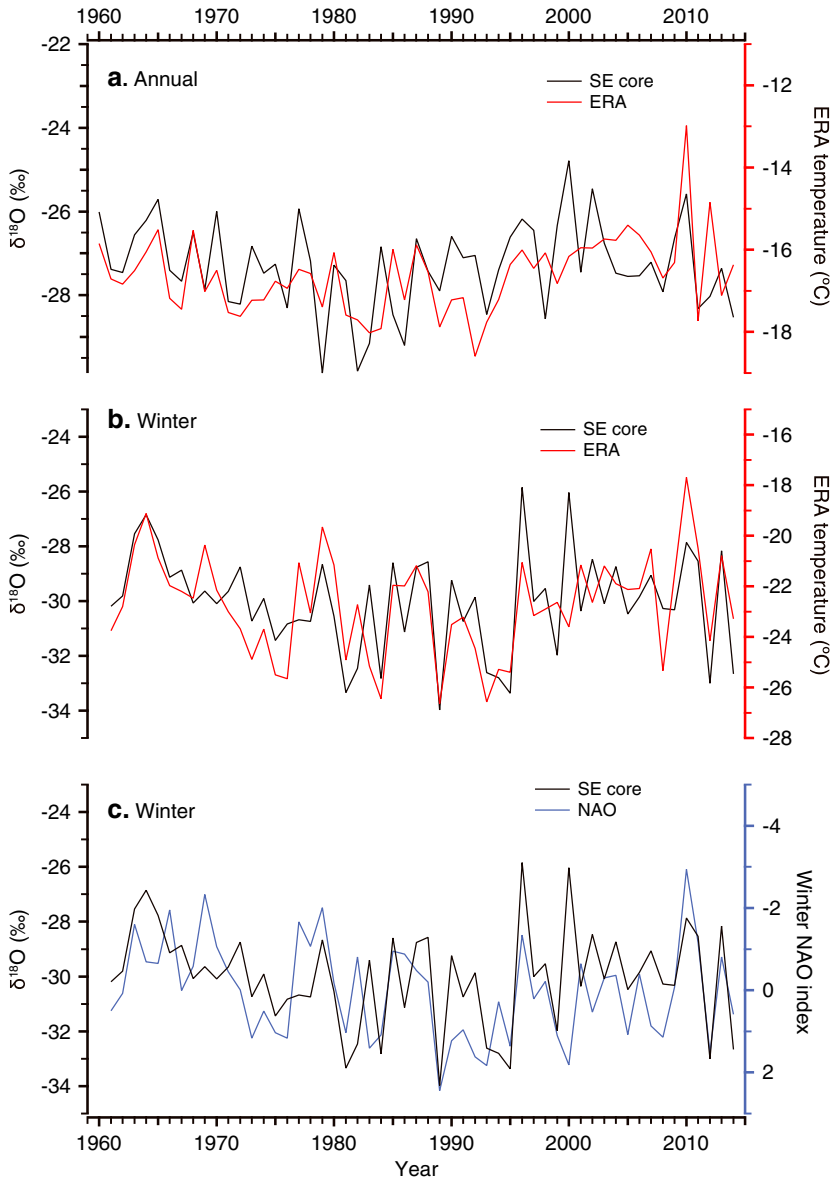

Figure 8. Annual and winter $\delta^{18}O$ in the SE-Dome core, air temperature, and NAO index. (a) Annual mean $\delta^{18}O$ in the SE-Dome core and air temperature from ERA-40-I. (b) The same as in Figure 8a but for winter. Winter is defined as December of the last year to February of the current year (i.e., the 1980 winter is the period from December. 1979 to February 1980). (c) Winter $\delta^{18}O$ in the SE-Dome core and the winter NAO index (Hurrell, 2003).

amount from ERA-40-I, because it is reconstructed directly from the thickness of the ice layers (Figure 9). Furthermore, in the models, the correlation between $\delta^{18}O$ and the monthly accumulation is weak (r = 0.08–0.20), suggesting that a minor impact of the precipitation amount on $\delta^{18}O$. Therefore, the high correlation of the $\delta^{18}O$ values in the SE-Dome core and models does not guarantee the accuracy of the precipitation amounts in the models.

The reconstructed annual accumulation rate during 1960–2014 was 1.02 ± 0.21 m yr^{-1} (average ± standard deviation) (Table 3). The seasonal accumulation rate shows no seasonal difference: 0.25 ± 0.07 m, 0.25 ± 0.09 m, 0.27 ± 0.09 m, and 0.25 ± 0.07 m for spring, summer, autumn, and winter, respectively (Table 3). The high snow accumulation without significant seasonality in the SE-Dome core suggests that this coring location is ideal for preserving the past environmental changes with minimum biases of seasonality.

The annual accumulation rate shows an increase with a slope of 3.6 mm yr^{-1} from 1960 to 2014 (r = 0.28, $p < 0.05$) (Figure 10). The autumn accumulation rate also shows a clear increasing trend with a slope of

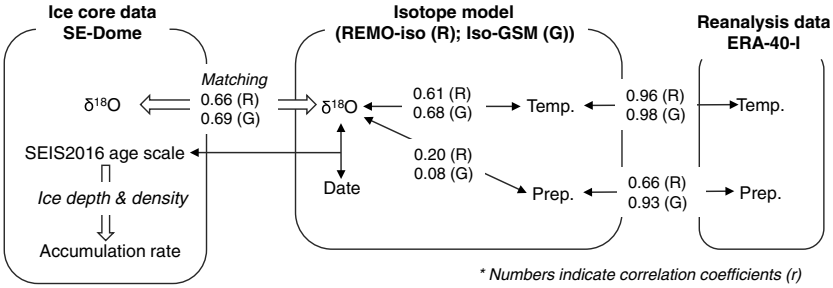

Figure 9. Schematic relationship among the SE-Dome, isotope model (REMO-iso and iso-GSM), and ERA-40-I data. The numbers indicate correlation coefficients, *r*, for REMO-iso (R) and for iso-GSM (G).

2.6 mm yr^{-1} (r = 0.46, $p < 0.01$). The winter accumulation rate also has an increase with a slope of 1.2 mm yr^{-1}, although the significance is low (r = 0.25, $p < 0.10$). Interestingly, there is no significant increasing (nor decreasing) trend in the other two seasons. The increasing annual accumulation rate is therefore mainly caused by the autumn accumulation rate.

The ERA-40-I precipitation amount during 1960–2014 bears a strong similarity to the accumulation data from the SE-Dome core. First, the average precipitation amount in ERA-40-I during 1960–2014 of 0.98 ± 0.22 m yr^{-1} agrees well with the reconstructed annual accumulation rate from the SE-Dome core (Table 3). Second, the interannual correlations are statistically significant for the annual, autumn, and winter records (Table 3 and Figure 10). Finally, the increasing trends (1960–2014) of the accumulation rates found in the SE-Dome data are consistent with those in the ERA-40-I precipitation data for the annual (3.5 mm yr^{-1}) and autumn (2.1 mm yr^{-1}) records (Figure 10).

This increasing accumulation rate is likely linked to the decrease in Arctic sea ice area in summer and autumn due to global warming (e.g., Vihma, 2014). The increase in precipitation is explained by an enhanced local evaporation due to sea ice retreat (Bintanja & Selten, 2014) and a reinforced poleward moisture transport (Zhang et al., 20136). A quantitative breakdown of the origin of increases in Arctic precipitation in projected 21st century is estimated to 60% by local evaporation (peaking in late autumn and winter) and 40% by the remote moisture transport (peaking in summer and early autumn) (Bintanja & Selten, 2014). Thus, the increasing accumulation rates in autumn and winter in the SE-Dome record suggest that the enhanced hydrological cycle probably caused by the decrease in Arctic sea ice area.

Regarding the precipitation amount in summer and winter, there are significant disagreements between the SE-Dome core and ERA-40-I data. In summer, the estimated accumulation from the SE-Dome data, 0.25 ± 0.09 m yr^{-1}, is larger than that of the ERA-40-I data, 0.17 ± 0.06 m yr^{-1}. On the other hand, in winter, the SE-Dome accumulation of 0.25 ± 0.07 m yr^{-1} is smaller than the ERA-40-I value, 0.32 ± 0.12 m yr^{-1}. This mismatch cannot be explained by sublimation of the SE-Dome core, because the large summer accumulation of SE-Dome data contradicts the possible bias caused by sublimation loss during summer. The uncertainty of the SEIS2016 age scale either cannot explain the mismatch because (1) the shorter summer (or longer winter) length in the SE-Dome core creates other mismatches in the neighboring lengths of spring and autumn, during which the SE-Dome accumulation and ERA-40-I precipitation are consistent, and (2) the SE-Dome $\delta^{18}O$ and ERA-40-I temperature are significantly correlated in all seasons (Table 2 and section 3.4.), implying the validity of the SEIS2016 age scale. Therefore, the disagreement suggests that the ERA-40-I data

Table 3
Accumulation Rates Based on the SE-Dome Ice Core Data and ERA-40-I Precipitation and the Correlation Coefficients of Their Comparisons

	Annual	Spring (MAM)	Summer (JJA)	Autumn (SON)	Winter (DJF)
Accumulation based on SE-Dome core data (m yr^{-1})	1.02 ± 0.21	0.25 ± 0.07	0.25 ± 0.09	0.27 ± 0.09	0.25 ± 0.07
Precipitation from ERA-40-I (m yr^{-1})	0.98 ± 0.22	0.23 ± 0.10	0.17 ± 0.06	0.26 ± 0.10	0.32 ± 0.12
Correlation between SE accumulation and ERA-40-I (r)	0.65***	0.15 (ns)	0.21(ns)	0.51***	0.39***

Note. ns: not significant.
***$p < 0.01$.

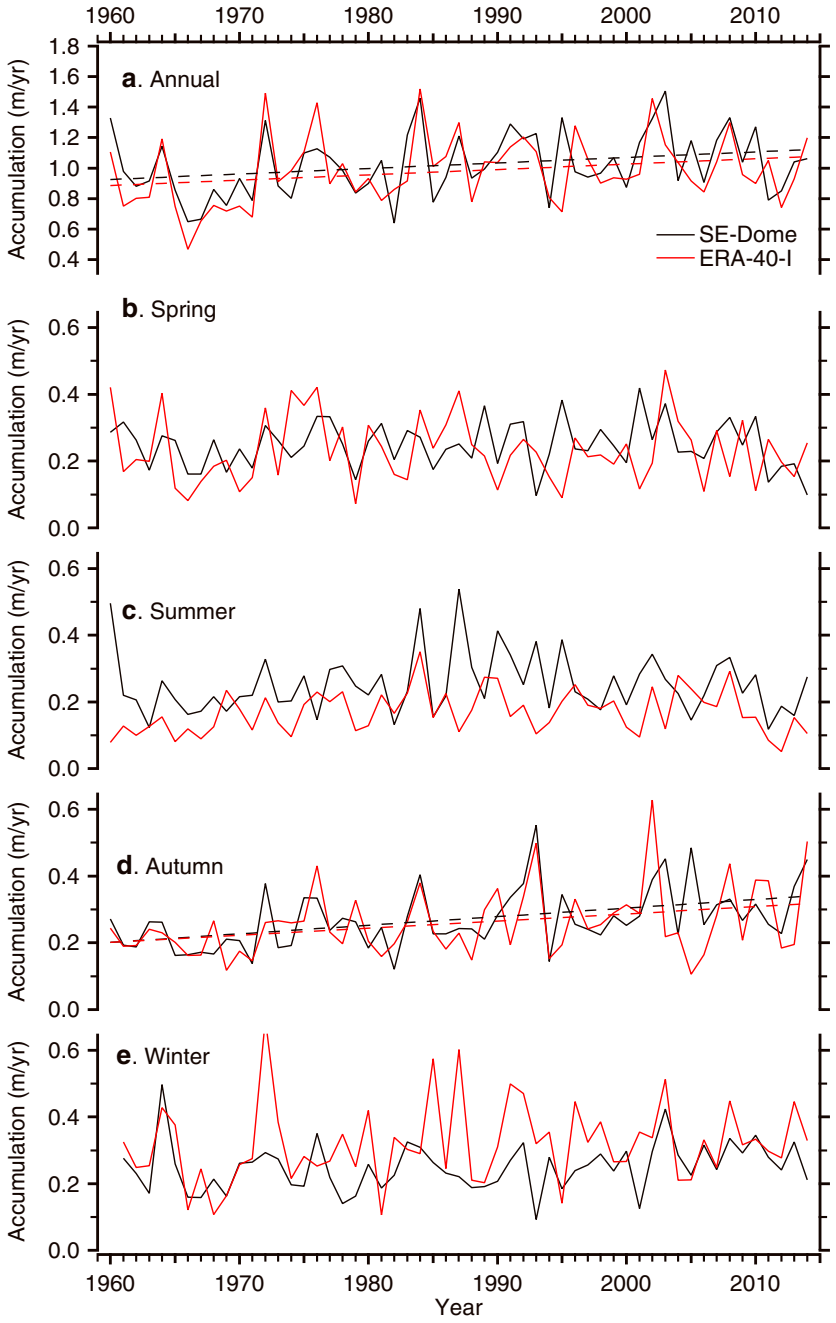

Figure 10. Snow accumulation rate reconstructed from the SE-Dome core and ERA precipitation data. (a) Annual snow accumulation rate from the SE-Dome core (black; m year^{-1}) and ERA-40-I precipitation data (red). (b–e) The same as in Figure 10a but for spring (March–May), summer (June–August), autumn (September–November), and winter (December of the last year to February), respectively. The dotted lines indicate the linear regression lines for the SE-Dome data (black) and ERA-40-I (red).

underestimate the precipitation amount during summer by 38% and overestimate it during winter by 28% at the SE-Dome location.

The biased stronger seasonality in the ERA-40-I data would result from characteristics of the forecasting models of ERAs mainly because of sparse meteorological observation points in Greenland. Note that the ERA-40-I data reproduced a strong seasonality, summer minimum, and winter maximum in precipitation, at Tasiilaq meteorological station (25 m asl; Figure 1) (Cappelen et al., 2001) 190 km away from the SE-Dome region. Therefore, we argue that precise reproduction of weather near SE-Dome region appears to be difficult

partly because of its complex and steep topography. In the future, those uncertainties can be reduced by a high-resolution climate model (Satoh et al., 2014) and developments of technique such as data assimilation of precipitation (Lien et al., 2013).

3.6. Limitations and Advantages of Isotope Matching Dating

The dating method using isotope matching can only be applied to the period for which the isotope simulation data are available, which is typically after the 1970s but can potentially be extended to the late 19th century using historical weather simulations (Compo et al., 2011; Yoshimura, 2015). Although this method may not be applicable to alpine glacier cores where significant surface melt occurs, it can be applied to ice cores drilled at high snow accumulation sites, where the postdepositional processes are insignificant. Ice cores from alpine glaciers are promising targets because they often suffer from unclear $\delta^{18}O$ seasonal cycles (e.g., Shiraiwa et al., 2002; Yasunari et al., 2007). Precise time scales with monthly time resolution would provide valuable atmospheric environmental data from ice cores, such as on black carbon (e.g., McConnell et al., 2007), radiogenic aerosols (e.g., Beer et al., 1988), and stable isotopes of nitrate and sulfate (e.g., Geng et al., 2014).

Potentially, this method can be more widely applicable to other sites and water-isotope based climate proxies (e.g., corals, tree ring cellulose, and speleothem) using a proxy system model (Dee et al., 2015; Evans et al., 2013), which calculates a complete set of forward physical processes (Evans et al., 2013). Even for ice cores drilled at low snow accumulation sites, it would be possible to model $\delta^{18}O$ diffusion and other postdepositional processes such as sublimation or exchange with water vapor (Steen-Larsen et al., 2014; Town et al., 2008; Hoshina et al., 2014, 2016). The proxy system modeling has been used for data assimilation-based reconstructions using a global network of ice cores as well, though the temporal resolution is still annual scale (Steiger et al., 2017). The method is developing rapidly, and a recent study showed that the proxy data, rather than reconstructed environmental information, can be assimilated directly for climate reconstructions (Okazaki & Yoshimura, 2017). In summary, with the help of proxy system modeling, the dating method based on isotope matching will give accurate chronology for these archives and subsequently also provide precise data for accumulation rate or growth rate for each material archives.

4. Conclusions

We have presented a new $\delta^{18}O$ record from an ice core obtained in southeast Greenland at SE-Dome. The SE-Dome core is dated based on pattern matching of the $\delta^{18}O$ variations between the ice core record and a simulated template. The accuracy of the SEIS2016 age scale is confirmed by multiple age markers. The precision of the age scale is approximately a few months during 1960–2014. Our analyses suggest that the winter 1995/1996 did not produce a $\delta^{18}O$ minimum because of a combination of warm air temperature, weak moisture transport, and cooler SST in the moisture source region.

The precise age scale provides a reliable record of snow accumulation rates during 1960–2014 at SE-Dome. The reconstructed annual accumulation rate increases with a slope of 3.6 (mm yr^{-1}), which is mainly caused by the increase in the autumn accumulation rate (2.6 mm yr^{-1}). This increasing accumulation rate is likely linked to the enhanced hydrological cycle caused by the decrease in Arctic sea ice area. Our reconstructed accumulation implies that the ERA reanalysis data underestimate the accumulation in summer by 38% and overestimate it in winter by 28% at the dome site. However, this discrepancy could be due to small-scale variations in the region not represented by the reanalysis/models.

There is no seasonality of the accumulation rate, suggesting that seasonally unbiased climate records can be retrieved. Minimum effects of postdepositional processes are also expected because of the high accumulation rate (1.02 ± 0.21 m yr^{-1}). The SE-Dome is therefore an ideal site for retrieving the past climate history. The SEIS2016 age scale provides a basis for forthcoming data on inorganic and organic aerosols, stable isotopes of nitrate and sulfate, and radiogenic nuclides from the SE-Dome core.

Acknowledgments
We are grateful to the drilling and initial analysis teams of the SE-Dome ice core. We thank Shohei Hattori of the Tokyo Institute of Technology and Hotaek Park of the JAMSTEC for discussions. The ERA-40 and ERA-interim data were provided courtesy of ECMWF. This study was supported by the MEXT/JSPS KAKENHI (grant 26257201 and 16K12573): the Joint Research Program of the Institute of Low Temperature Science, Hokkaido University: and the Readership Program of the Institute of Low Temperature Science, Hokkaido University. This study is partly responsible for ArCS (Arctic Challenge for Sustainability Project; PI Shin Sugiyama). The data used in this study will be available in Hokkaido University Collection of Scholarly and Academic papers (http://hdl.handle.net/2115/67128) and also in National Climatic Data Center, NOAA (https://www.ncdc.noaa.gov/data-access/paleoclimatology-data/datasets).

References

Alley, R. B., Shuman, C. A., Meese, D. A., Gow, A. J., Taylor, K. C., Cuffey, K. M., … Elder, B. (1997). Visual-stratigraphic dating of the GISP2 ice core: Basis, reproducibility, and application. *Journal of Geophysical Research*, *102*, 26,367–26,381. https://doi.org/10.1029/96JC03837

Arienzo, M. M., McConnell, J. R., Chellman, N., Criscitiello, A. S., Curran, M., Fritzsche, D., … Steffensen, J. P. (2016). A method for continuous ^{239}Pu determinations in Arctic and Antarctic ice cores. *Environmental Science & Technology*, *50*, 7066–7073. https://doi.org/10.1021/acs.est.6b01108

Beer, J., Siegenthaler, U., Bonani, G., Finkel, R. C., Oeschger, H., Suter, M., & Wölfli, W. (1988). Information on past solar activity and geomagnetism from ^{10}Be in the Camp Century ice core. *Nature*, *331*, 675–679. https://doi.org/10.1038/331675a0

Berggren, A. M., Beer, J., Possnert, G., Aldahan, A., Kubik, P., Christl, M., … Vinther, B. M. (2009). A 600-year annual ^{10}Be record from the NGRIP ice core, Greenland. *Geophysical Research Letters*, *36*, L11801. https://doi.org/10.1029/2009GL038004

Bintanja, R., & Selten, F. M. (2014). Future increases in Arctic precipitation linked to local evaporation and sea-ice retreat. *Nature*, *509*, 479–482. https://doi.org/10.1038/nature13259

Cappelen, J., Jørgensen B. V., Laursen E. V., Stannius L. S., & Thomsen R. S. (2001). The observed climate of Greenland, 1958-1999 with climatological Standard Normals, 1961–1990, Danish Meteorological Institute, Technical report 00–18, ISSN 1399–1388.

Clausen, H. B., & Hammer, C. U. (1988). The Laki and Tambora eruptions as revealed in Greenland ice cores from 11 locations. *Annals of Glaciology*, *10*, 16–22.

Compo, G. P., Whitaker, J. S., Sardeshmukh, P. D., Matsui, N., Allan, R. J., Yin, X., … Worley, S. J. (2011). The Twentieth Century Reanalysis Project. *Quarterly Journal of the Royal Meteorological Society*, *137*, 1–28. https://doi.org/10.1002/qj.776

Climate Prediction Center (1996), Special climate summary 96/1: Climate conditions during the 1995–1996 northern hemisphere winter, March 1996, NOAA/NWS/NCEP/CPC. Retrieved from http://www.cpc.ncep.noaa.gov/products/special_summaries/96_1/

Dansgaard, W. (1964). Stable isotopes in precipitation. *Tellus*, *16*, 436–468. https://doi.org/10.1111/j.2153-3490.1964.tb00181.x

Dee, D. P., Uppala, S. M., Simmons, A. J., Berrisford, P., Poli, P., Kobayashi, S., … Vitart, F. (2011). The ERA-Interim reanalysis: Configuration and performance of the data assimilation system. *Quarterly Journal of the Royal Meteorological Society*, *137*, 553–597. https://doi.org/10.1002/qj.828

Dee, S., Emile-Geay, J., Evans, M. N., Allam, A., Steig, E. J., & Thompson, D. M. (2015). PRYSM: An open-source framework for PRoxY System Modeling, with applications to oxygen-isotope systems. *Journal of Advances in Modeling Earth Systems*, *7*, 1220–1247. https://doi.org/10.1002/2015MS000447

Dhomse, S. S., Emmerson, K. M., Mann, G. W., Bellouin, N., Carslaw, K. S., Chipperfield, M. P., … Thomason, L. W. (2014). Aerosol microphysics simulations of the Mt. Pinatubo eruption with the UM-UKCA composition-climate model. *Atmospheric Chemistry and Physics*, *14*, 11,221–11,246. https://doi.org/10.5194/acp-14-11221-2014

Dibb, J. E., Whitlow, S. I., & Arsenault, M. (2007). Seasonal variations in the soluble ion content of snow at Summit, Greenland: Constraints from three years of daily surface snow samples. *Atmospheric Environment*, *41*, 5007–5019. https://doi.org/10.1016/j.atmosenv.2006.12.010

Evans, M. N., Tolwinski-Ward, S. E., Thompson, D. M., & Anchukaitis, K. J. (2013). Applications of proxy system modeling in high resolution paleoclimatology. *Quaternary Science Reviews*, *76*(15), 16–28. https://doi.org/10.1016/j.quascirev.2013.05.024

Gao, C., Robock, A., & Ammann, C. (2008). Volcanic forcing of climate over the past 1500 years: An improved ice core-based index for climate models. *Journal of Geophysical Research*, *113*, D23111. https://doi.org/10.1029/2008JD010239

Geng, L., Cole-Dai, J., Alexander, B., Erbland, J., Savarino, J., Schauer, A. J., … Zatko, M. C. (2014). On the origin of the occasional spring nitrate peak in Greenland snow. *Atmospheric Chemistry and Physics*, *14*, 13,361–13,376. https://doi.org/10.5194/acp-14-13361-2014

Hammer, C. U., Clausen, H. B., & Dansgaard, W. (1980). Greenland ice sheet evidence of post-glacial volcanism and its climatic impact. *Nature*, *288*, 230–235.

Holdsworth, G., Pourchet, M., Prantl, F. A., & Meyerhof, D. P. (1984). Radioactivity levels in a firn core from the Yukon Territory, Canada. *Atmospheric Environment*, *18*, 461–466.

Hoshina, Y., Fujita, K., Iizuka, Y., & Motoyama, H. (2016). Inconsistent relationships between major ions and water stable isotopes in Antarctic snow under different accumulation environments. *Polar Science*, *10*, 1–10. https://doi.org/10.1016/j.polar.2015.12.003

Hoshina, Y., Fujita, K., Nakazawa, F., Iizuka, Y., Miyake, T., Hirabayashi, M., … Motoyama, H. (2014). Effect of accumulation rate on water stable isotopes of near-surface snow in inland Antarctica. *Journal of Geophysical Research: Atmospheres*, *119*, 274–283. https://doi.org/10.1002/2013JD020771

Hurrell, J. (2003). NAO Index Data provided by the Climate Analysis Section, NCAR, Boulder, USA, Updated regularly. Accessed 30 Jan. 2017.

Iizuka, Y., Matoba, S., Yamasaki, T., Oyabu, I., Kadota, M., & Aoki, T. (2016). Glaciological and meteorological observations at the SE-Dome site, southeastern Greenland Ice Sheet. *Bulletin of Glaciological Research*, *34*, 1–10. https://doi.org/10.5331/bgr.15R03

Iizuka, Y., Miyamoto, A., Hori, A., Matoba, S., Furukawa, R., Saito, T., … Takeuchi, N. (2017). A firn densification process in the high accumulation dome of southeastern Greenland. *Arctic, Antarctic, and Alpine Research*, *49*, 13–27. https://doi.org/10.1657/AAAR0016-034

Iizuka, Y., Uemura, R., Motoyama, H., Suzuki, T., Miyake, T., Hirabayashi, M., & Hondoh, T. (2012). Sulphate–climate coupling over the past 300,000 years in inland Antarctica. *Nature*, *490*, 81–84. https://doi.org/10.1038/nature11359

Kanamitsu, M., Ebisuzaki, W., Woollen, J., Yang, S. K., Hnilo, J. J., Fiorino, M., & Potter, G. L. (2002). NCEP-DOE AMIP-II Reanalysis (R-2). *Bulletin of the American Meteorological Society*, *83*, 1631–1643. https://doi.org/10.1175/BAMS-83-11-1631

Koerner, R. M. (1997). Some comments on climatic reconstructions from ice cores drilled in areas of high melt. *Journal of Glaciology*, *43*, 90–97. https://doi.org/10.3198/1997JoG43-143-90-97

Lien, G., Kalnay, E., & Miyoshi, T. (2013). Effective assimilation of global precipitation: simulation experiments. *Tellus A*, *65*, 19915. https://doi.org/10.3402/tellusa.v65i0.19915

Masson-Delmotte, V., Steen-Larsen, H. C., Ortega, P., Swingedouw, D., Popp, T., Vinther, B. M., … White, J. W. C. (2015). Recent changes in north-west Greenland climate documented by NEEM shallow ice core data and simulations, and implications for past-temperature reconstructions. *The Cryosphere*, *9*, 1481–1504. https://doi.org/10.5194/tc-9-1481-2015

McConnell, J. R., Edwards, R., Kok, G. L., Flanner, M. G., Zender, C. S., Saltzman, E. S., … Kahl, J. D. W. (2007). 20th-century industrial black carbon emissions altered arctic climate forcing. *Science*, *317*, 1381–1384. https://doi.org/10.1126/science.1144856

Meese, D. A., Gow, A. J., Alley, R. B., Zielinski, G. A., Grootes, P. M., Ram, K., … Bolzan, J. F. (1997). The Greenland Ice Sheet Project 2 depth-age scale: Methods and results. *Journal of Geophysical Research*, *102*, 26,411–26,423. https://doi.org/10.1029/97JC00269

Okazaki, A., Satoh, Y., Tremoy, G., Viemux, F., Scheepmaker, R. A., & Yoshimura, K. (2015). Interannual variability of isotopic composition in water vapor over West Africa and its relation to ENSO. *Atmospheric Chemistry and Physics*, *15*, 3193–3204. https://doi.org/10.5194/acp-15-3193-2015

Okazaki, A., & Yoshimura, K. (2017). Development and evaluation of a system of proxy data assimilation for paleoclimate reconstruction. *Climate of the Past*, *13*, 379–393. https://doi.org/10.5194/cp-13-379-2017

Paillard, D., Labeyrie, L., & Yiou, P. (1996). Macintosh program performs time-series analysis. *EOS Transactions of the American Geophysical Union*, *77*, 379. https://doi.org/10.1029/96EO00259

Plummer, C. T., Curran, M. A. J., van Ommen, T. D., Rasmussen, S. O., Moy, A. D., Vance, T. R., … Mayewski, P. A. (2012). An independently dated 2000-yr volcanic record from Law Dome, East Antarctica, including a new perspective on the dating of the 1450s CE eruption of Kuwae, Vanuatu. *Climate of the Past*, *8*, 1929–1940. https://doi.org/10.5194/cp-8-1929-2012

Rasmussen, S. O., Andersen, K. K., Svensson, A. M., Steffensen, J. P., Vinther, B. M., Clausen, H. B., … Ruth, U. (2006). A new Greenland ice core chronology for the last glacial termination. *Journal of Geophysical Research*, *111*, D06102. https://doi.org/10.1029/2005JD006079

Risi, C., Noone, D., Worden, J., Frankenberg, C., Stiller, G., Kiefer, M., … Sturm, C. (2012). Process-evaluation of tropospheric humidity simulated by general circulation models using water vapor isotopologues: 1. Comparison between models and observations. *Journal of Geophysical Research*, *117*, D05303. https://doi.org/10.1029/2011JD016621

Sakai, A., Nuimura, T., Fujita, K., Takenaka, S., Nagai, H., & Lamsal, D. (2015). Climate regime of Asian glaciers revealed by GAMDAM Glacier Inventory. *The Cryosphere*, *9*, 865–880. https://doi.org/10.5194/tc-9-865-2015

Satoh, M., Tomita, H., Yashiro, H., Miura, H., Kodama, C., Seiki, T., … Kubokawa, H. (2014). The Non-hydrostatic Icosahedral Atmospheric Model: description and development. *Progress in Earth and Planetary Science*, *1*, 18. https://doi.org/10.1186/s40645-014-0018-1

Scholz, D., & Hoffmann, D. L. (2011). StalAge—An algorithm designed for construction of speleothem age models. *Quaternary Geochronology*, *6*, 369–382. https://doi.org/10.1016/j.quageo.2011.02.002

Shiraiwa, T., Kohshima, S., Uemura, R., Yoshida, N., Matoba, S., Uetake, J., & Godoi, M. A. (2002). High net accumulation rates at Campo de Hielo Patagónico Sur, South America, revealed by analysis of a 45.97 m long ice core. *Annals of Glaciology*, *35*, 84–90. https://doi.org/10.3189/172756402781816942

Sjolte, J., Hoffmann, G., Johnsen, J., Vinther, B. M., Masson-Delmotte, V., & Sturm, C. (2011). Modeling the water isotopes in Greenland precipitation 1959–2001 with the meso-scale model REMO-iso. *Journal of Geophysical Research*, *116*, D18105. https://doi.org/10.1029/2010JD015287

Steen-Larsen, H. C., Masson-Delmotte, V., Hirabayashi, M., Winkler, R., Satow, K., Prié, F., … Sveinbjörnsdottír, A. E. (2014). What controls the isotopic composition of Greenland surface snow? *Climate of the Past*, *10*, 377–392. https://doi.org/10.5194/cp-10-377-2014

Steiger, N. J., Steig, E. J., Dee, S. G., Roe, G. H., & Hakim, G. J. (2017). Climate reconstruction using data assimilation of water isotope ratios from ice cores. *Journal of Geophysical Research: Atmospheres*, *122*, 1545–1568. https://doi.org/10.1002/2016JD026011

Sturm, K., Hoffmann, G., Langmann, B., & Stichler, W. (2005). Simulation of $\delta^{18}O$ in precipitation by the regional circulation model REMOiso. *Hydrological Processes*, *19*, 3425–3444. https://doi.org/10.1002/hyp.5979

Svensson, A., Andersen, K. K., Bigler, M., Clausen, H. B., Dahl-Jensen, D., Davies, S. M., … Vinther, B. M. (2008). A 60,000 year Greenland stratigraphic ice core chronology. *Climate of the Past*, *4*, 47–57. https://doi.org/10.5194/cp-4-47-2008

Town, M. S., Warren, S. G., Walden, V. P., & Waddington, E. D. (2008). Effect of atmospheric water vapor on modification of stable isotopes in near-surface snow on ice sheets. *Journal of Geophysical Research*, *113*, D24303. https://doi.org/10.1029/2008JD009852

Uemura, R., Matsui, Y., Yoshimura, K., Motoyama, H., & Yoshida, N. (2008). Evidence of deuterium excess in water vapour as an indicator of ocean surface conditions. *Journal of Geophysical Research*, *113*, D19114. https://doi.org/10.1029/2008JD010209

Uemura, R., Yonezawa, N., Yoshimura, K., Asami, R., Kadena, H., Yamada, K., & Yoshida, N. (2012). Factors controlling isotopic composition of precipitation on Okinawa Island, Japan: Implications for paleoclimate reconstruction in the East Asian Monsoon region. *Journal of Hydrology*, *475*, 314–322. https://doi.org/10.1016/j.jhydrol.2012.10.014

Uppala, S. M., Kållberg, P. W., Simmons, A. J., Andrae, U., Da Costa Bechtold, V., Fiorino, M., … Woollen, J. (2005). The ERA-40 re-analysis. *Quarterly Journal of the Royal Meteorological Society*, *131*, 2961–3012. https://doi.org/10.1256/qj.04.176

Vihma, T. (2014). Effects of Arctic sea ice decline on weather and climate: A review. *Surveys in Geophysics*, *35*, 1175–1214. https://doi.org/10.1007/s10712-014-9284-0

Vinther, B. M., Johnsen, S. J., Andersen, K. K., Clausen, H. B., & Hansen, A. W. (2003). NAO signal recorded in the stable isotopes of Greenland ice cores, *Geophysical Research Letters*, *30*(30), 1387. https://doi.org/10.1029/2002GL016193

Vinther, B. M., Jones, P. D., Briffa, K. R., Clausen, H. B., Andersen, K. K., Dahl-Jensen, D., & Johnsen, S. J. (2010). Climatic signals in multiple highly resolved stable isotope records from Greenland. *Quaternary Science Reviews*, *29*, 522–538. https://doi.org/10.1016/j.quascirev.2009.11.002

Wei, Z., Yoshimura, K., Okazaki, A., Ono, K., Kim, W., Yokoi, M., & Lai, C.-T. (2016). Understanding the variability of water isotopologues in near-surface atmospheric moisture over a humid subtropical rice paddy in Tsukuba, Japan. *Journal of Hydrology*, *533*, 91–102. https://doi.org/10.1016/j.jhydrol.2015.11.044

White, J. W. C., Barlow, L. K., Fisher, D., Grootes, P., Jouzel, J., Johnsen, S. J., … Clausen, H. (1997). The climate signal in the stable isotopes of snow from Summit, Greenland: Results of comparisons with modern climate observations. *Journal of Geophysical Research*, *102*, 26,425–26,439. https://doi.org/10.1029/97JC00162

Whitlow, S., Mayewski, P. A., & Dibb, J. E. (1992). A comparison of major chemical-species seasonal concentration and accumulation at the South-Pole and Summit, Greenland. *Atmospheric Environment*, *26*, 2045–2054. https://doi.org/10.1016/0960-1686(92)90089-4

Yasunari, T. J., Shiraiwa, T., Kanamori, S., Fujii, Y., Igarashi, M., Yamazaki, K., … Hondoh, T. (2007). Intra-annual variations in atmospheric dust and tritium in the North Pacific region detected from an ice core from Mount Wrangell, Alaska. *Journal of Geophysical Research*, *112*, D10208. https://doi.org/10.1029/2006JD008121

Yoshimura, K. (2015). Stable water isotopes in climatology, meteorology, and hydrology: A review. *Journal of the Meteorological Society of Japan*, *93*, 513–533. https://doi.org/10.2151/jmsj.2015-036

Yoshimura, K., Frankenberg, C., Lee, J., Kanamitsu, M., Worden, J., & Röckmann, T. (2011). Comparison of an isotopic AGCM with new quasi global satellite measurements of water vapor isotopologues. *Journal of Geophysical Research*, *116*, D19118. https://doi.org/10.1029/2011JD016035

Yoshimura, K., Kanamitsu, M., Noone, D., & Oki, T. (2008). Historical isotope simulation using reanalysis atmospheric data. *Journal of Geophysical Research*, *113*, D19108. https://doi.org/10.1029/2008JD010074

Zhang, X., He, J., Zhang, J., Polyakov, I., Gerdes, R., Inoue, J., & Wu, P. (2013). Enhanced poleward moisture transport and amplified northern high-latitude wetting trend. *Nature Climate Change*, *3*, 47–51. https://doi.org/10.1038/nclimate1631